

# DETERMINING NOISE TEMPERATURES IN BEAMWAVEGUIDE SYSTEMS

*W. Imbriale, W. Veruttipong, T. Otsoshi, and M. Franco*

Jet Propulsion Laboratory

California Institute of Technology

Pasadena, CA 91109

## ABSTRACT

A new 34-meter research and development antenna was fabricated and tested as a precursor to introducing **beamwaveguide** antennas and **Ka-band** frequencies into the NASA/JPL Deep Space Network. For deep space use, system noise temperature is a critical parameter. There are thought to be two major contributors to noise temperature in a BWG system: the **spillover** past the mirrors and the conductivity loss in the walls. **However**, to date, there are no generally accepted methods for computing noise temperatures in a **beamwaveguide** system. An extensive measurement program was **undertaken** to determine noise temperatures in such a system along with a correspondent effort in analytic prediction. Utilizing a very sensitive radiometer, noise temperature measurements were made at the **cassegrain** focus, an intermediate focal point, and the focal point in the basement pedestal room. Several different horn diameters were used to simulate different amounts of **spillover** past the mirrors. Two analytic procedures were developed for computing noise temperature, one

utilizing circular waveguide modes and the other a semi-empirical approach. The results of both prediction methods are compared to the experimental data.

## 1. INTRODUCTION

Noise temperature due to a **beamwaveguide (BWG)** system is one of the major contributors to antenna receive system noise, especially for an ultra-low noise system or a **system** with high **spillover** power in the **BWG** shroud. A reasonably accurate prediction of the BWG noise temperature is essential. Direct analytical computation of the noise temperature of elaborate BWG systems, including all mirrors, is an extremely complex problem and, to date, there is no generally accepted method. This report presents two new techniques-one a purely analytical method and the second a semi-empirical approach,

The analytical method extends the approach of [ 1 ], which computes the waveguide modes that are propagating in the oversized **waveguides**. Reference [1] describes a PO integration procedure of the currents on the BWG mirrors using a Green's function appropriate to the circular waveguide geometry. Once all the modes in the waveguide are known, it is a simple matter to use standard approximations to determine the attenuation constant and thus the conductivity loss if the conductivity of the wall material is known. Also, all energy that propagates toward but spills past a BWG mirror is assumed to be lost in the walls of the **BWG** as **well**. The noise temperature is computed assuming both loss components see ambient temperature.

The second method uses a technique that combines an analytical approach with data from measurements to construct a specific expression to compute the BWG noise temperature.

To validate both approaches, a series of measurements were made on 1> S- 13, the recently completed research and development 34-meter BWG antenna (see Figs. 1 and 2). The experiments consisted of making very accurate noise temperature measurements for different gain horns located at both the cassegrain focus (f1) and the BWG focus of the upper portion of the BWG system (f2) (designed to image the horn at the cassegrain optics focal point). This portion of the BWG optics is enclosed in 2.44-meter (8-foot) diameter tube. By taking measurements at both focal points, the noise temperature of the BWG portion of the optics can be accurately determined. The results of both computation methods are compared to the measured data.

## 2. WAVEGUIDE MODE THEORY

The BWG tube analysis is conceptually similar to the physical optics (PO) analysis used in reflector antenna analysis.

The currents induced in the BWG mirror are obtained using a standard physical optics approximation of  $J = 2\hat{n} \times H_{inc}$  where  $\hat{n}$  is the surface normal and  $H_{inc}$  is the incident field. The difference from a standard PO analysis is 1) the method by which the incident field on a mirror is calculated, and 2) the method by which the scattered field is calculated.

One approach to calculating the scattered fields is to use a dyadic Green's formulation<sup>[1]</sup> where the field scattered from a BWG mirror are computed using the Green's function appropriate to the cylindrical waveguide geometry.

While it is conceptually convenient to use Green's functions to discuss the comparison with PO, the actual computation using this approach is rather cumbersome. Rather, a simpler method, based upon the reciprocity theorem, is used to calculate the waveguide fields. The basic problem is to find the fields radiated by an arbitrary current (the PO currents on the reflector) in a cylindrical waveguide. The problem is easily solved by expanding the radiated field in terms of a suitable set of normal modes with amplitude coefficients determined by an application of the Lorentz Reciprocity theorem.

An arbitrary field in a waveguide can be represented as an infinite sum of the normal modes for the guide. Let the normal modes be represented by

$$\begin{aligned}\bar{E}_n^{(\pm)} &= (\bar{e}_n \pm \bar{e}_{in})e^{\mp \gamma_n z} \\ \bar{H}_n^{(\pm)} &= (\pm \bar{h}_n + \bar{h}_{in})e^{\mp \gamma_n z}\end{aligned}\tag{1}$$

where  $\bar{E}_n^{(+)}$  represents a mode traveling in the +z direction and  $\bar{E}_n^{(-)}$  is a mode traveling in the -z direction. For the basic normal mode description, see for example Harrington<sup>[2]</sup>.

Let the field radiated in the positive z direction by the current be represented by

$$\begin{aligned}
\bar{E}^{(+)} &= \sum_{\mathbf{n}} a_{\mathbf{n}} \bar{E}_{\mathbf{n}}^{(+)} \\
\bar{H}^{(+)} &= \sum_{\mathbf{n}} \frac{a_{\mathbf{n}}}{Z_{\mathbf{n}}} \bar{H}_{\mathbf{n}}^{(+)}
\end{aligned} \tag{2}$$

and the field radiated in the negative  $z$  direction by

$$\begin{aligned}
\bar{E}^{(-)} &= \sum_{\mathbf{n}} b_{\mathbf{n}} \bar{E}_{\mathbf{n}}^{(-)} \\
\bar{H}^{(-)} &= \sum_{\mathbf{n}} \frac{b_{\mathbf{n}}}{Z_{\mathbf{n}}} \bar{H}_{\mathbf{n}}^{(-)}
\end{aligned} \tag{3}$$

Recalling the Lorentz Reciprocity theorem, if  $\bar{E}_1, \bar{H}_1$ , and  $\bar{E}_2, \bar{H}_2$  are the fields due to  $\bar{J}_1, \bar{J}_2$ , respectively, then

$$\int_V \hat{n} \cdot [\bar{E}_1 \times \bar{H}_2 - \bar{E}_2 \times \bar{H}_1] ds = \int_V [\bar{E}_2 \bullet \bar{J}_1 - \bar{E}_1 \bullet \bar{J}_2] dV \tag{4}$$

If we let  $E_l, H_l$  be the fields due to the sources  $J$  and  $E_{\mathbf{n}}^{\pm}, H_{\mathbf{n}}^{\pm}$  be the modal (source-free) solutions, substituting in the Lorentz Reciprocity theorem gives

$$-\int_V \left[ \bar{E}_{\mathbf{n}}^{(\pm)} \times \bar{H}_1 - \bar{E}_1 \times \frac{\bar{H}_{\mathbf{n}}^{\pm}}{Z_{\mathbf{n}}} \right] \bullet \hat{n} ds = \int_V \bar{E}_{\mathbf{n}}^{(\pm)} \bullet J dV \tag{5}$$

We choose as our volume that bounded by the perfectly conducting guide walls and the two cross-sectional planes  $S_1$  and  $S_2$  (see Fig. 3). Then

$$\begin{aligned}
& \int_s \int_{s_1} (-\hat{z}) \cdot \left[ \bar{E}^{(-)} \times \frac{\bar{H}_n^{(\pm)}}{Z_n} - \bar{E}_n^{(\pm)} \times H^{(-)} \right] ds \\
& + \int_{s_2} (\hat{z}) \cdot \left[ \bar{E}^{(+)} \times \frac{\bar{H}_n^{(\pm)}}{Z_n} - \bar{E}_n^{(\pm)} \times \bar{H}^{(+)} \right] ds
\end{aligned} \tag{6}$$

Note that the integral along the wall doesn't contribute because on  $S_3$   
 $\hat{n} \cdot \bar{E}_1 \times \bar{H}_2 = \bar{H}_2 \cdot \hat{n} \times \bar{E}_1 = \bar{H}_2 \cdot \text{Tangential } \bar{E} = 0$  for both  $E^{(*)}$  or  $E_n^{(\pm)}$ .

Also only transverse fields enter into computations because  $\hat{z} \cdot \bar{E} \times \bar{H}$  selects transverse components.

For the normal mode function  $E_n^+, H_n^+$  it is readily found that

$$\int_s = -\frac{2b_n}{Z_n} \tag{7}$$

when the expansion for  $E^+$  and  $E^-$  are used in conjunction with the orthogonal property and

$$\int_s (\bar{e}_n \times \bar{h}_m) \cdot \hat{z} ds = \begin{cases} 0 & \text{if } n \neq m \\ 1 & \text{if } m = n \end{cases} \tag{8}$$

Also, if we use the normal mode function  $\bar{E}_n^{(-)}, \bar{H}_n^{(-)}$  we find that

$$\int_s = -2 \frac{a_n}{Z_n} \tag{9}$$

We have therefore shown that

$$\begin{aligned} a_n &= -\frac{1}{2} Z_n \int_V [\bar{E}_n^{(-)} \cdot \bar{J}] dV \\ b_n &= -\frac{1}{2} Z_n \int_V [\bar{E}_n^{(+)} \cdot \bar{J}] dV \end{aligned} \quad (10)$$

Since we have only surface currents, the integral for the PO currents is over the surface of the reflector. If we let

$$c_n = -\frac{1}{2} \int_s J_s \cdot \bar{E}_n^{(-)} ds \quad (11)$$

where  $J_s$  is the physical optics currents on the mirror, then

$$\begin{aligned} \bar{H}^+ &= \sum_n c_n \bar{H}_n^{(-)} \\ \bar{E}^{(+)} &= \sum_n Z_n c_n \bar{E}_n^{(-)} \end{aligned} \quad (12)$$

and the total power contained in the fields is

$$P = \sum_n z_n |c_n|^2 \quad (13)$$

The physical optics currents induced on the first mirror are computed either in the standard way if the spillover past the mirror is small (i.e., >25 dB edge taper) by utilizing the free-space near-field radiating H field of the horn and  $J_s = 2\hat{n} \times H_{inc}$  or by utilizing a technique similar to the one just described to compute the propagating modes from the horn and radiating in the oversized

waveguide and also utilizing the appropriate H field derived from these modes as the incident field. Physical optics currents on subsequent mirrors are computed from the H field derived from the propagating waveguide modes. The technique is summarized in Fig. 4, where it should be noted that

$$H = \int_s J_1 \cdot \overline{\overline{G}}_{ws} ds = \sum_n c_n \overline{H}_n^{(-)} \quad (14)$$

The power loss in the conductor is obtained utilizing the standard technique to compute the power dissipated in the conductor per unit length (see [2]) as

$$P_d(Z) = R \int_0^{2\pi} |\overline{H}_t|^2 a d\phi \quad (15)$$

where

$$R = \sqrt{\frac{\omega\mu}{2\sigma}} \quad (16)$$

and  $\sigma$  is the wall conductivity,  $a$  the radius, and  $\overline{H}_t^2$  the tangential H field. It should be noted that  $P_d$  is a function of  $Z$  since  $\overline{H}_t^2$  is a function of  $Z$  (i.e., it is composed of more than one waveguide mode).

The power loss is computed from

$$P = P_0 e^{-2\alpha d} \quad (17)$$

where  $d$  is the distance from  $Z_1$  to  $Z_2$  and the attenuation constant is computed as



$$\alpha d = \frac{\int_{z_1}^{z_2} P_d(Z) dZ}{2P_f} \quad (18)$$

where  $P_f$  is the power flow in the waveguide.

To compute noise temperature it is convenient to separate the total RF power, originating from the horn aperture (viewed in transmission, for convenience) and propagating into two parts

$$P_{BWG} = P_m + P_{spill} \quad (19)$$

where  $P_{spill}$  is the portion that spills past the mirrors (since the mirrors do not fill the waveguide).  $P_{spill}$  can be computed for each mirror by integrating the total power radiated from the induced mirror currents and comparing it to the incident power. Note that the computation uses the induced currents derived from the waveguide modes. It is then assumed that this **spillover** power sees ambient temperature since it would be lost in the tube due to multiple bounces in a **lossy** material.

The total noise temperature then is composed of two parts-the noise due to the **spillover** power added to the noise from the attenuation of  $P_m$  due to the conductivity loss.

### 3. SEMI-EMPIRICAL APPROACH

A noise temperature of elaborate BWG systems including BWG mirrors and shroud can also be computed by using a new technique that combines an analytical approach with data from measurement tests to construct a specific expression to compute the BWG noise temperature. This technique begins by separating the total RF power, originating from a horn aperture (viewed in transmission, for convenience) and propagating through a BWG shroud ( $P_{BWG}$ ), into two parts (see Fig. 5)

$$P_{BWG} = P_m + P_{spill} \quad (20)$$

where  $P_m$  is the majority of the total power that is always confined inside all 13WG mirrors; it does not contact the BWG wall and there are no multiple reflection, diffraction, and creeping wave components.  $P_m$  can be computed easily and accurately because all BWG wall and mirror interactions are not included. It should be noted that in the analysis, the mirrors are assumed to **radiate** in free space, Thus the  $P_{spill}$  from this analysis is different from the  $P_{spill}$  of the waveguide mode theory.  $P_{spill}$  is the sum of **spillover** powers of each mirror. It creeps and bounces around the BWG walls, mirrors, brackets (behind the mirrors), and edges, etc., and suffers dissipation loss and consequent noise. **On an average**, the  $P_{spill}$  power largely dissipates before a small remainder exits the BWG opening near f1 (see Fig. 2). Even though  $P_{spill}$  can be computed accurately ( $P_{spill} = P_{BWG} - P_m$ ), its field distribution and its chaotic behavior inside the **lossy** BWG is virtually impossible to compute analytically.

From Eq. (20), the corresponding noise temperatures are

$$T_{BWG} = T_m + T_{spill} \quad (21)$$

where  $T_{BWG}$  is the total noise temperature (in kelvins) due to the BWG system (including the shroud, mirror, brackets, etc.). The values  $T_m$  and  $T_{spill}$  are the noise temperature contributions from  $P_m$  and  $P_{spill}$ , respectively. Because of the simplicity of  $P_m$ , its corresponding noise temperature  $T_m$  can be computed with acceptable accuracy. For 6061T6 aluminum with conductivity of  $2.3 \times 10^7$  mho/meter and 270-K physical temperature, the noise temperature  $T_m$  at X-band (8.45 GHz) is (see [3])

$$T_m = 0.734 \frac{P_m}{P_{BWG}} = 0.734 a_m \quad (22)$$

where  $a_m$  is the  $P_m$  fraction of  $P_{BWG}$ , dimensionless.

The noise temperature due to spillover power  $P_{spill}$  is given in a very simple form as

$$T_{spill} = \left( \frac{P_1}{P_{BWG}} \right) T_1 + \left( \frac{P_2}{P_{BWG}} \right) T_2 = \alpha_1 T_1 + \alpha_2 T_2 \quad (23)$$

where  $P_1$  is the total spillover power of the two mirrors (M5 and M6) in the basement and the value  $P_2$  is the total spillover power of the four mirrors (M1, M2, M3, and M4) above the basement ceiling. The values  $\alpha_1$  and  $\alpha_2$  are the normalized powers (with respect to  $P_{BWG}$ ) of  $P_1$  and  $P_2$ , respectively.

By substituting Eqs. (22) and (23) into Eq. (21), the BWG noise temperature at X-band becomes

$$T_{\text{BWG}} = 0.734a_m + \alpha_1 T_1 + \alpha_2 T_2 \quad (24)$$

By performing various measurements at the NASA DSN BWG research station at Goldstone, the coefficients  $T_1$  and  $T_2$  at X-band have been obtained<sup>[3]</sup>.

No basement shroud	$T_1 = 300 \pm 10 \text{ K}$	(25)
	$T_2 = 240 \pm 45 \text{ K}$	

Full shroud	$T_1 = 280 \pm 20 \text{ K}$	(26)
	$T_2 = 230 \pm 45 \text{ K}$	

Figure 6 shows the comparison between predicted and measured BWG noise temperatures for various **total spillover** powers at X-band. The results indicate a very good agreement, especially in the operating range ( $0.5\% \leq P_{\text{spill}} \leq 1.2\%$ ).

#### 4. MEASUREMENTS PROGRAM

Figure 1 shows a recent photograph of the 34-m-diameter BWG antenna built at the **NASA/JPL** Goldstone tracking facility near Barstow, California. This antenna is the first antenna built for NASA of the BWG type and is primarily an **R&D** antenna. One of the uses of this antenna has been to develop and verify theoretical models that can be used as tools for designing future improved BWG antennas.

Focal points **f1**, **f2**, and **f3** are depicted in Fig. 2. Focal point **f1** is the **cassegrain** focal point near the main reflector vertex. An **intermediate** focal **f2** lies above the azimuth track, and focal point **f3** is the final BWG focal point located in a subterranean pedestal room. Degradations caused by the BWG system mirrors and shrouds were determined from comparisons made of operating system noise temperatures measured at the different focal points.

As discussed earlier, the goal of the experimental technique was to determine the degradations caused by the noise temperature contributions from wall losses and mirror **spillovers** in the BWG system. The experimental technique that was conceived and implemented involved measurements of operating system noise temperature at **f1**, **f2**, and **f3**. Taking the difference of the noise temperatures measured at **f1** and **f2** gives the information on the total losses of the BWG system that include (1) dissipative losses due to finite conductivity of four mirrors, (2) **spillover losses** associated with four mirrors, and (3) shroud wall losses between **f1** and **f2**. Similarly, information of the total losses of the remaining two mirrors, shroud walls, and unshrouded path between **f2** and **f3** are determined from **differencing** noise temperatures measured at **f2** and **f3**.

To obtain information on the losses pertaining only to the **cassegrain** portion of the BWG antenna, the experimental procedure involved making an operating system noise temperature' measurement first with the test package on the ground, and then making a measurement with the test package installed at **f1**. The difference between **f1** and ground *noise* temperatures reveals the amount of degradation **casued** by **spillover** of power from the horn into the region between the **subreflector** and main reflector, scattering from the tripod legs, noise

contribution from illumination of the ground and sky region as seen from the **subreflector** focus, and leakage through gaps between panels and perforations in the main reflector surfaces, as well as noise temperature due to illuminating the area between the horn aperture and **BWG** shroud walls.

For the experimental technique to yield the information described above, it was required that the absolute noise temperature at the different test locations be accurate to about  $\pm 0.5$  K and be repeatable to about  $\pm 0.2$  K. The accuracy of values obtained for differential measurements is estimated to be  $\pm 0.3$  K and is more accurate than absolute values due to common errors canceling each other out in the differencing process.

In order to achieve these goals, an ultra-stable radiometer was required and the test package required **good** mechanical stability after installation at the various focal points. It was shown in a previous **report**<sup>[4]</sup> that a number of measurements were made with the test packages installed at the different **focal** points, then going back to the ground, and then back to the different focal points. Such repeatability tests confirmed that the X-band test package and **radiometric** system met the accuracy requirements stated above for making absolute and differential noise temperature measurements.

Figures 7 and 8 show the X-band test package installed at **f1** and **f3**. Horns of different gains at **f1** and **f2** were achieved easily by beginning with the **29-dBi** horn and systematically removing horn sections to produce a lower gain horn. At both **f1** and **f3**, test package adjustments were used to align the phase centers for the different gain horns to the desired geometric focal points.

Special radiometric calibration techniques were employed such as ( 1 ) correcting for changes in atmospheric noise contributions due to changes in air temperature and relative humidity, and (2) performing periodic real-time calibrations of radiometric system for measuring noise temperatures. Further details of the microwave performance of these test packages and radiometric techniques used to achieve the desired stability and precision have been reported elsewhere<sup>[5]</sup>.

## 5. RESULTS

The measurements described above were made at cassegrain focus  $f_1$ , at the intermediate focus  $f_2$ , and at the basement focus  $f_3$ .

For contrasting the two theories, the most interesting measurements were those made at  $f_2$ , since the shroud surrounds the mirrors. Since there is no shroud in the pedestal room, both methods give the same result for the basement mirrors.

A horn pattern input at  $f_2$  is imaged at  $f_1$  so measurements made with the same horn gain at  $f_1$  and  $f_2$  can be difference to give the noise temperature due only to the BWG portion of the system. A plot of the measured data for the upper BWG ( $f_2$  to  $f_1$ ) is compared to both theories in Fig. 9 for horn gains from 25 to 29.8 dB. Obviously the lower gain horn spills more energy past the mirrors and has a higher noise temperature contribution. Interestingly, both methods do a fairly good job of predicting the noise temperatures. For reference, the BWG system was designed to operate with the 29.8-dB gain horn.

## 6. ACKNOWLEDGMENTS

The research described in this paper was carried out by the Jet Propulsion Laboratory, California Institute of Technology, under a contract with the National Aeronautics and Space Administration.

## 7. REFERENCES

1. Cha, A.G. and Imbriale, W.A. (1992) A new analysis of beamwaveguide antennas considering the presence of the metal enclosure IEEE Transactions on Antennas and Propagation, Vol. 40, No. 9, pp. 1041-1046.
2. Barrington, R.F. (1961) Time-Harmonic Electromagnetic Fields, McGraw Hill, Chapter 8.
3. Veruttipong, W. and France, M. (1993) A technique for computation of noise temperature due to a beamwaveguide shroud, 1993 IEEE AP-S International Symposium, The University of Michigan, Ann Arbor, Michigan.
4. Bathker, D.A., Veruttipong, W., Otoshi, T. Y., and Cramer, Jr., P.W. (1992) Beamwaveguide antenna performance predictions with comparisons to experimental results, Microwave Theory and Techniques, Special Issue (Microwaves in Space), Vol. MTT-40, No. 6, pp. 1274-1285,
5. Otoshi, T. Y., Stewart, S. R., and France, M.M. (1992) Portable microwave test packages for beamwaveguide antenna performance evaluations, Microwave Theory and Techniques, Special Issue (Microwaves in Space), Vol. MTT-40, No. 6, pp. 1286--1293.



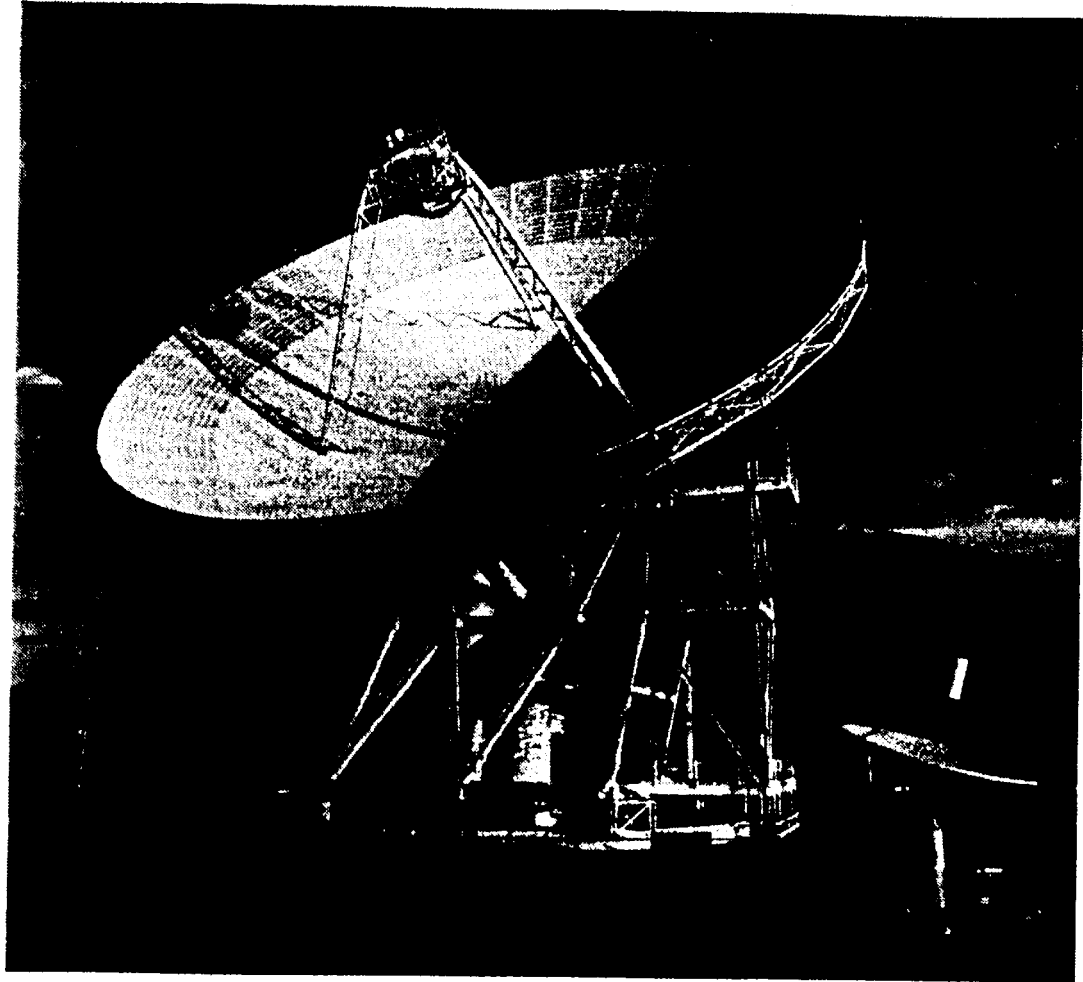


Figure 1. DSS- 13 34-meter BWG antenna.

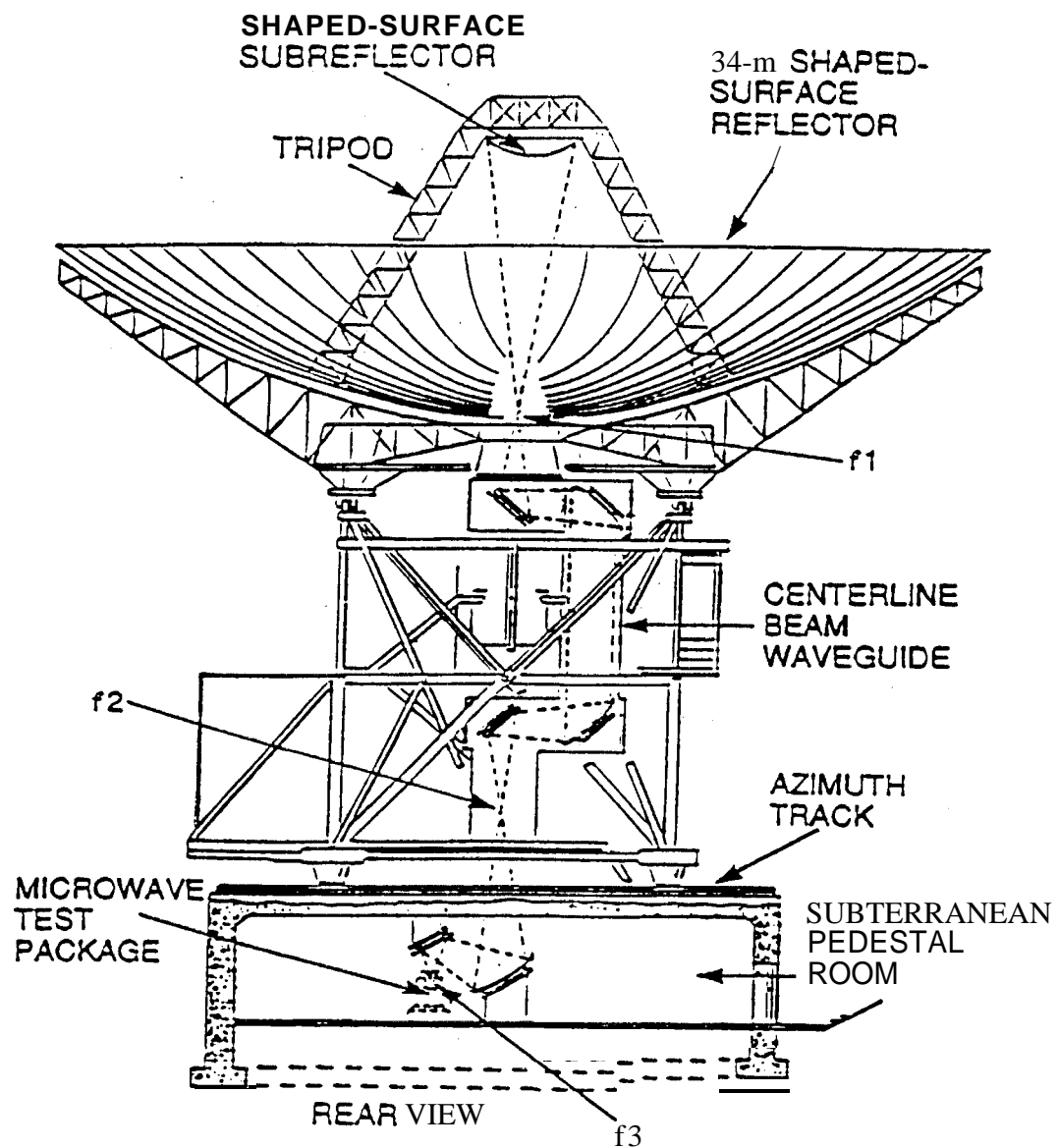


Figure 2. 34-m BWG antenna focal points.

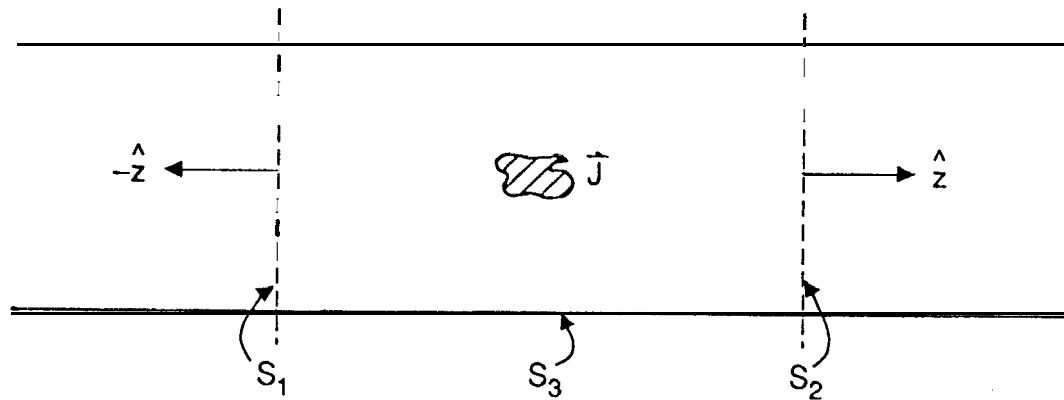


Figure 3. Geometry for computing waveguide modes.

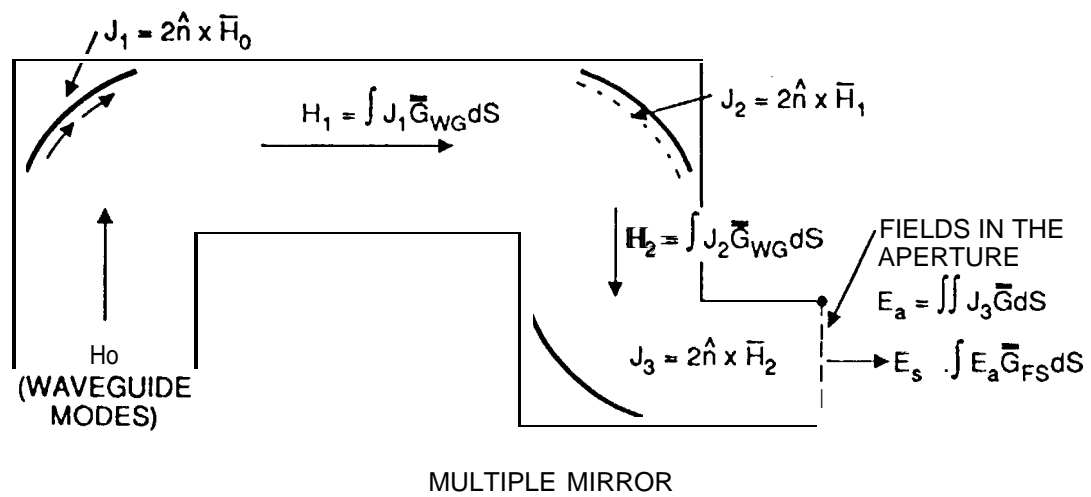


Figure 4. Computation of fields in the BWG system.

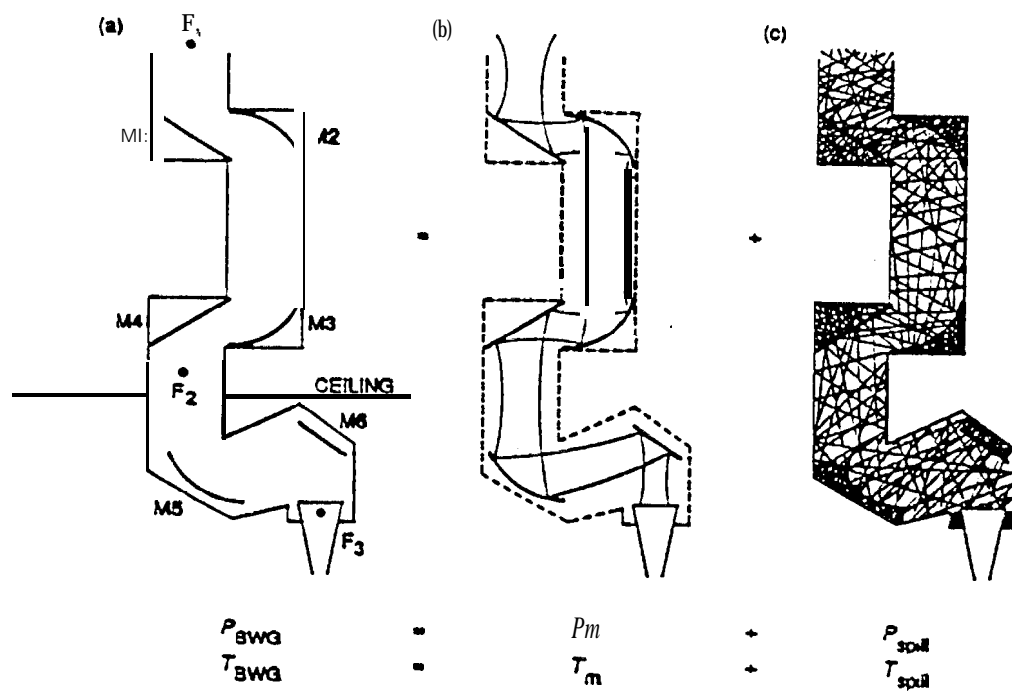


Figure 5. Characteristics of the fields inside a BWG shroud and their corresponding noise temperatures.

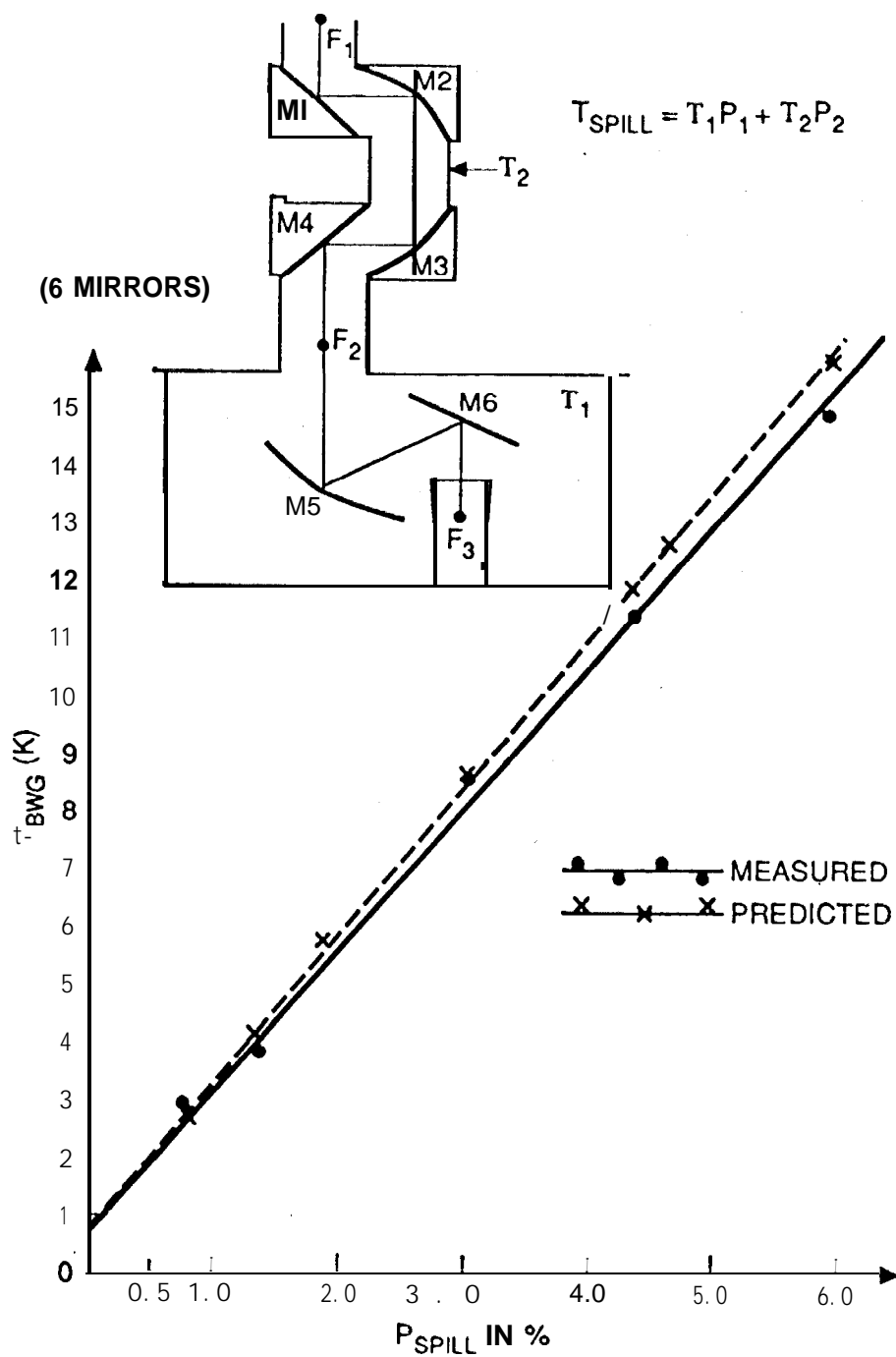


Figure 6. The comparison between predicted and measured BWG noise temperatures at X-band.

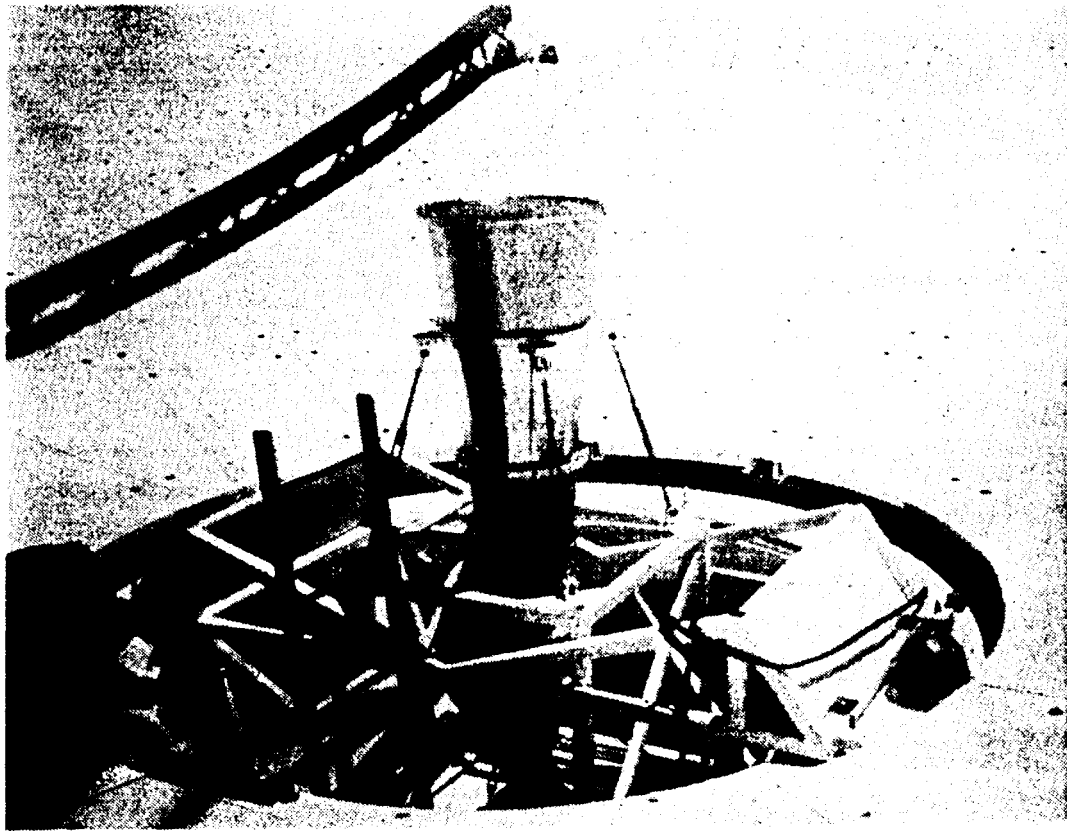


Figure 7. Partial view of the X-band 29-dBi horn test package and mounting structure installed at the cassegrain focal point  $f_1$ .

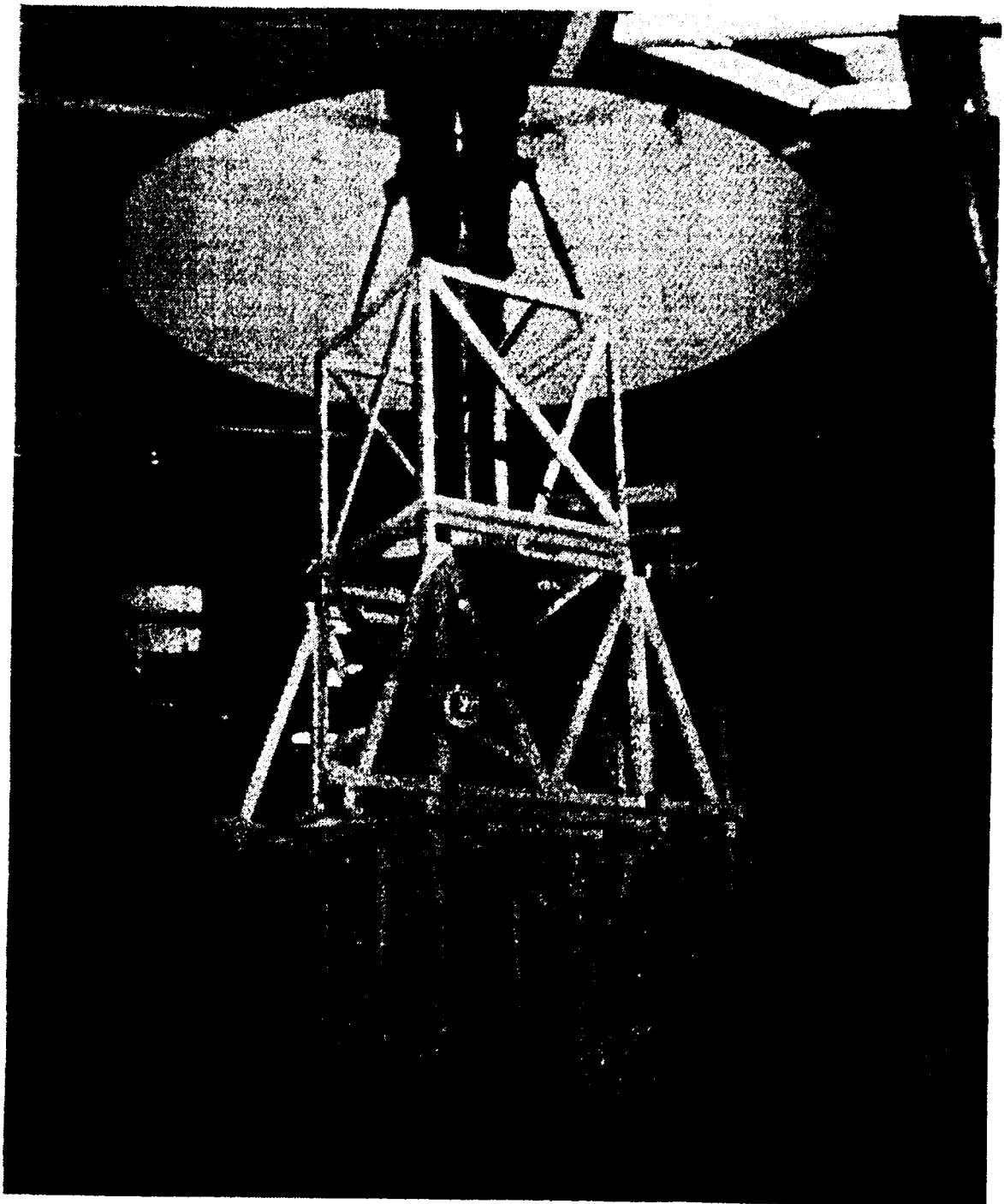


Figure 8. X-band 22-dBi horn test package and mounting table installed in the pedestal room focal point f3.

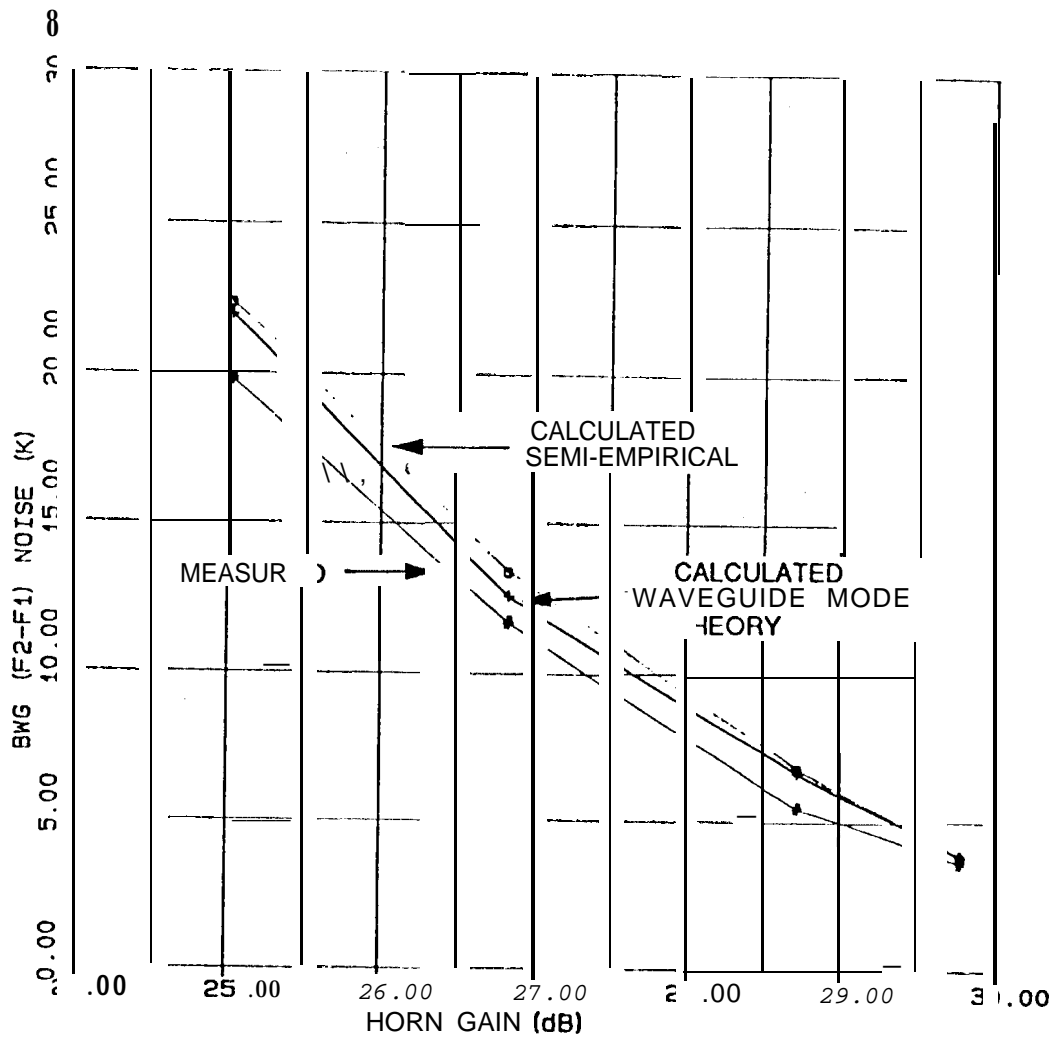


Figure 9. Comparison of computed and measured noise temperatures with different feedhorn gains at  $f_2$ .